metals

MDPI

Article

A Comparative Study on Mechanical and Corrosion Behaviours of $\alpha/(\alpha + \beta)$ Mg-Li Alloys Subjected to Ultrasonic Nanocrystal Surface Modification

Yun Zou, Shuhao Liu, Qilong Wang and Yang Li *

School of Mechanical and Power Engineering, Zhengzhou University, Zhengzhou 450001, China; yunzou@zzu.edu.cn (Y.Z.); shuhaoliuzzu@163.com (S.L.); wangql@163.com (Q.W.)
* Correspondence: yangli@zzu.edu.cn

Abstract: Ultrasonic nanocrystal surface modification (UNSM) was applied to hot-rolled Mg-Li alloys (LAE361 and LA106). The microstructure, mechanical properties, deformation mechanisms, and corrosion resistance properties of these alloys after UNSM treatment were systematically studied. Significant improvement in surface hardness and decrease in surface roughness were achieved by UNSM treatment. Meanwhile, the basal texture intensity of the Mg-Li alloys reduced significantly, and several deformation twins appeared on the surface layer. The α phase of the surface layer underwent twin deformation and basal plane slip. The fibre textures in the β phase of LA106 Mg-Li alloy changed from γ and η to α and ε, which mainly resulted in the dislocation slip. More importantly, UNSM treatment exhibited enhanced strength and improved plasticity of LAE361 and LA106 Mg-Li alloys. The corrosion current density of LAE361 Mg-Li alloy reduced approximately 29.3% by UNSM treatment, while it increased the corrosion current density of LA106 Mg-Li alloy by 189.7%. These studies show that the application of UNSM to improve the corrosion resistance of duplex phases of LA106 Mg-Li alloy needs further investigation.

Keywords: Mg-Li alloys; ultrasonic nanocrystal surface modification; deformation mechanisms; microstructure; corrosion resistance

Citation: Zou, Y.; Liu, S.; Wang, Q.; Li, Y. A Comparative Study on Mechanical and Corrosion Behaviours of $\alpha/(\alpha + \beta)$ Mg-Li Alloys Subjected to Ultrasonic Nanocrystal Surface Modification. *Metals* **2022**, *12*, 681. https://doi.org/10.3390/met12040681

Academic Editors: Gilda Renna and Claudia Barile

Received: 10 March 2022
Accepted: 12 April 2022
Published: 15 April 2022

1. Introduction

Mg-Li alloys have been widely used in the aerospace, vehicle, and medical fields due to their low density, specific stiffness, and ease of recycling [1–4]. With the increase of material performance requirements, the low strength and poor corrosion resistance of Mg-Li alloys restrict their promotion and application. Therefore, developing Mg-Li alloys with high strength and ductility accompanied by good corrosion resistance is highly urgent.

Traditional methods, such as alloying [5,6], severe plastic deformation (SPD) [7], and coating [8] are used to improve the strength or corrosion resistance of Mg alloys. Alloying easily introduces the second phase to accelerate the corrosion rate, general SPD cannot coordinate the relationship between plasticity and strength, and coating needs to consider the issues of binding force and life, both of which have certain limitations. Recently, surface severe plastic deformation (SSPD) technologies were proposed to alleviate the surface properties of materials via inducing gradient structure, thereby improving their mechanical properties and corrosion resistance. The SSPD technologies use high-energy media (such as water, pellets, and tool heads) to bombard the material surface continuously and cause SPD, e.g., shot peening (SP) [9–11], waterjet peening (WJP) [12,13], laser shock peening [14–16], surface mechanical grinding treatment (SMGT) [17–19], and UNSM [20–23]. To achieve excellent comprehensive mechanical and corrosion resistance properties, obtaining a smooth surface and deep hardening layer via SSPD technologies are indispensable. UNSM is an emerging ultrasonic-assisted surface modification method. It uses a combination of ultrasonic impact and static pressure extrusion to produce a severe

and uniform high-strain-rate plastic deformation on the surface of the metal, which is the ideal fine–coarse crystal gradient microstructure. The high strength of refined grains and the high plasticity of coarse grains can be effectively used to improve their comprehensive mechanical properties. Moreover, studies have reported that surface roughness has a significant effect on the corrosion resistance of materials. UNSM can produce samples with better surface roughness than that of SSPD treatments such as SP and WJP [10,13]. In addition, UNSM induces a thicker plastic deformation layer on the surface of the materials. The entire treatment process involves a simple operation and can be controlled accurately. Moreover, UNSM is an environmentally–friendly method.

UNSM was initially used to treat welds by eliminating the residual tensile stress at the welding location. Ye et al. [20] applied UNSM to 304 stainless steel welds and reported that this treatment transformed tensile stress into compressive residual stress. Moreover, UNSM simultaneously induced a phase transformation and refined the surface grains, thereby enhancing the surface hardness and corrosion resistance of metal materials. With further developments, UNSM was also applied to strengthen Mg alloys. Hou et al. [21] reported that the hardness, yield stress, and wear resistance of AZ31B Mg alloy were improved significantly by UNSM. However, compared to that of the untreated samples, the corrosion resistance of the alloy was not compromised. In another report, the corrosion resistance of AZ31B was improved due to the surface residual compressive stress and lower surface roughness value after UNSM [23].

At present, studies on the application of UNSM in Mg alloys focus on commercial Mg alloys, and the application mainly focuses on the processing of rod-like samples. However, few studies on the application of UNSM in Mg-Li alloys, especially the plates of Mg-Li alloys, were reported. The reason lies in the difficulty of sheet metal processing and the ease of producing bending deformation due to the lower strength of Mg-Li alloy. Therefore, two Mg-Li alloys of LAE361 and LA106 with different microstructures (single and duplex phases) and properties were selected for this paper, and the hot-rolled treatment was carried out to ensure the two Mg-Li alloys had sufficient strength for the subsequent UNSM treatment process. Finally, UNSM was expected to improve the mechanical and corrosion resistance properties of the Mg-Li alloy.

2. Materials and Methods

2.1. Materials and Processing

As-cast LAE361 and LA106 Mg-Li alloys provided by the Aluminum Corporation of China (Beijing, China) were selected as experimental materials. Their chemical compositions were determined by using a plasma emission spectrometer (ICAP 7200, Thermo Fisher Scientific, Waltham, MA, USA), as shown in Table 1.

Table 1. Chemical composition of two Mg-Li alloys.

Element Content	LAE361	LA106
Li (wt.%)	3.28	10.02
Al (wt.%)	5.12	5.69
Er (wt.%)	0.91	0.08
Mg (wt.%)	Balance	Balance

The two as-cast Mg-Li alloys were homogenized at 573 K for 12 h using a cooling water system before being hot-rolled. Then, samples were heated at 573 K for 30 min and rolled with 30% thickness reduction at 573 K. A 5% reduction was applied during each rolling pass. Before each rolling pass, the samples were heated at 573 K for 5 min to reduce the stress introduced by rolling. The hot-rolled samples were signed as HR for comparison. Subsequently, the samples were cut by using an electric discharge machine. The hot-rolled samples were ground by using 1500# grit sandpaper before UNSM treatment. Then, the hot-rolled samples were subjected to UNSM on both sides. Figure 1 shows the schematic diagram of the UNSM equipment and the involved procedure. During the treatment, the

ball continuously collides with the surface of samples by an ultrasonic vibration frequency of 28 kHz and an amplitude of 10 μm. The static pressure, interval, and moving speed were 0.3 MPa, 0.05 mm, and 1500 mm/min, respectively. UNSM was performed along the rolling direction (RD) of the hot-rolled sheet.

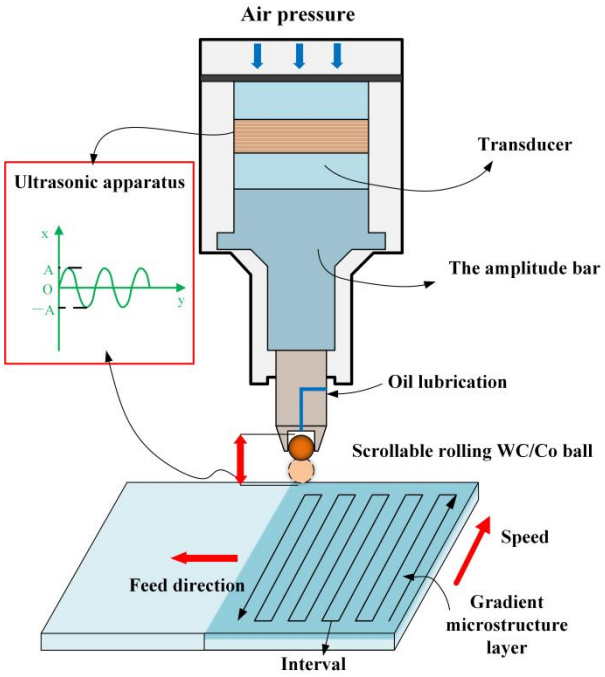

Figure 1. Schematic diagram of the UNSM instrument.

2.2. Microstructural Characterization

Samples were cut along the cross-section of the materials to observe the microstructure of the Mg-Li alloys. After mechanical polishing and washing, the Mg-Li alloys were etched using a 2–4 vol.% nitric acid alcohol solution. Then, the microstructure was observed by optical microscopy (OM) (VHX-2000, Keyence, Osaka, Japan).

X-ray diffraction (XRD) analysis of the specimens was measured by a PAnalytical Empyrean XRD system (Empyrean, Malvenpanako, NL, USA). The voltage and current were 40 kV and 30 mA, respectively. The diffraction angle (2θ) ranged from 20° to 80°. The data was analyzed by MDI jade 6.0 software (Materials Data, Livermore, CA, USA).

The surface roughness of the sample was measured using a three-dimensional surface topography measurement system (NPFLEX, Bruker, Karlsruhe, Germany) with a test area of 472 × 629 μm^2.

The textures of the Mg-Li alloys were tested by using the Schulz reflection method. Four incomplete pole figures of {0002} and $\{10\bar{1}0\}$, $\{10\bar{1}1\}$, and $\{10\bar{1}2\}$ of the α phase and three incomplete pole figures of {200}, {110}, and {211} of the β phase were scanned using the concentric circle-stepping mode. A high-resolution diffractometer (X'Pert PRO MRD) equipped with a texture goniometer was used. The measurement was performed by using Cu-K_α radiation and a Ni filter at a step size of 5°, and the scanned angle measurement ranges of the α and β phases were 0–70° and 0–360°, respectively. The texture analysis software MTEX was used to analyze the test data and calculate the pole figures.

2.3. Evaluation of Mechanical Properties

Microhardness tests were performed by using a microhardness tester (HV-1000, Beijing Times Mountain Peak Technology, Beijing, China) with a loading of 0.5 N and holding time of 10 s. The microhardness variations were measured along the vertical depth with an interval of 50 μm, and each position was measured five times.

The tensile mechanical property of the samples was investigated by using an MTS tension tester (MTS 370.02, MTS Systems Corporation, Eden Prairie, MI, USA) with a displacement rate of 1.5 mm/min. The gauge length, width, and thickness of the tensile specimens were 25, 10 and 2 mm, respectively. The tensile test of specimens was repeated at least three times. The morphology of the fractured surfaces was observed by using a scanning electron microscope (SEM) (Auriga-bu, Zeiss, Jena, Germany).

2.4. Corrosion Resistance Characterization

2.4.1. Electrochemical Test

The electrochemical test was performed using electrochemical impedance spectroscopy (EIS) and potentiodynamic polarization measurement by an electrochemical workstation (RST5200F, Zhengzhou SRIS Instrument Technology, Zhengzhou, China) in 3.5 wt.% NaCl solution at RT. The Mg-Li alloys were the working electrode (with an exposed area of 1 cm^2). A platinum electrode was used as the auxiliary electrode, and the saturated calomel electrode (SCE) was used as the reference electrode. First, the open circuit potential test was performed for 20 min. EIS was conducted in the frequency range 10^5–10^{-2} Hz with a voltage amplitude of 7 mV. The potentiodynamic polarization curve was obtained with a scan rate of 1 mV/s. Electrochemical tests were performed at least three times.

2.4.2. Hydrogen Evolution Test

The samples (with the exposed area of 1 cm^2) were immersed in a 3.5 wt.% NaCl solution for 48 h and the hydrogen evolution was recorded at certain times. Then, the surface morphology of the samples was observed using optical microscopy after the immersion.

3. Results

3.1. Microstructure

Figure 2 shows the cross-sectional microstructures of LAE361 and LA106 Mg-Li alloys before and after UNSM. LAE361 Mg-Li alloy exhibits α phase structure, whereas LA106 Mg-Li alloy exhibits a duplex phases structure (α + β). Notably, the samples showed a gradient microstructure with an SPD layer on the surface after the UNSM treatment. Consequently, several twin deformations appeared in the α phase near the surface layer, and the grains were refined.

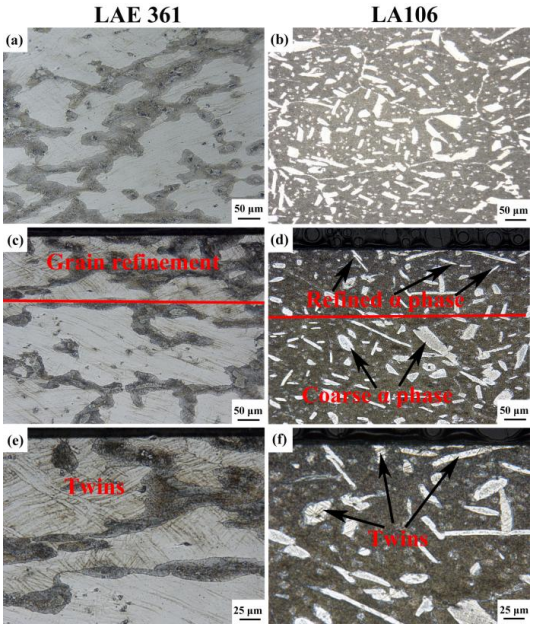

Figure 2. Microstructures of LAE361 and LA106 Mg-Li alloys before the UNSM treatment (**a**,**b**) and after the UNSM treatment (**c**–**f**).

XRD was used to study the effects of UNSM on the composition and phases of LAE361 and LA106 Mg-Li alloys. Figure 3 shows the XRD of the samples before and after UNSM. From the XRD peaks obtained before and after the UNSM treatment, it is evident that the phase compositions of LAE361 and LA106 Mg-Li alloys did not change. The phases of LAE361 Mg-Li alloy include α phase, AlLi phase, and Al_3Er phase. The phases of LA106 Mg-Li alloy include α phase, β phase, AlLi phase and Al_3Er phase.

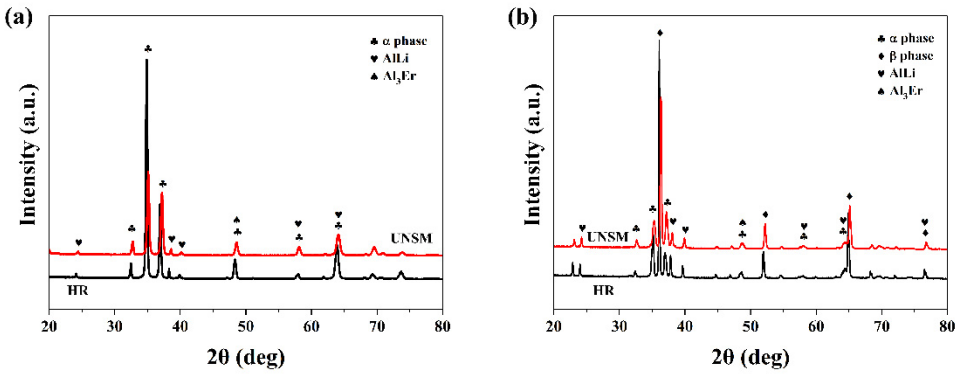

Figure 3. XRD patterns of LAE361 Mg-Li alloy (**a**) and LA106 Mg-Li alloy (**b**) before and after the UNSM treatment.

3.2. Surface Roughness

Figure 4 shows the 3D morphology of LAE361 and LA106 Mg-Li alloys before and after the UNSM treatment. Figure 4a,c clearly show that the sandpaper left many scratches on the sample after grinding. In contrast, Figure 4b,d show fewer scratches and traces of the UNSM treatment on the sample surface. Thus, it can be deduced that the SPD on the sample surface can remove the scratches and improve the surface roughness (Ra). Figure 4e shows the Ra of LAE361 and LA106 Mg-Li alloys before and after UNSM. The Ra of LAE361 and LA106 Mg-Li alloys before the UNSM treatment were 0.179 and 0.346 µm, respectively. After UNSM, the average Ra of LAE361 and LA106 Mg-Li alloys were found to be 0.143 and 0.236 µm, respectively. Thus, the average Ra values of LAE361 and LA106 Mg-Li alloys reduced by approximately 20% and 32%, respectively. Therefore, the UNSM treatment significantly improved the Ra of Mg-Li alloys.

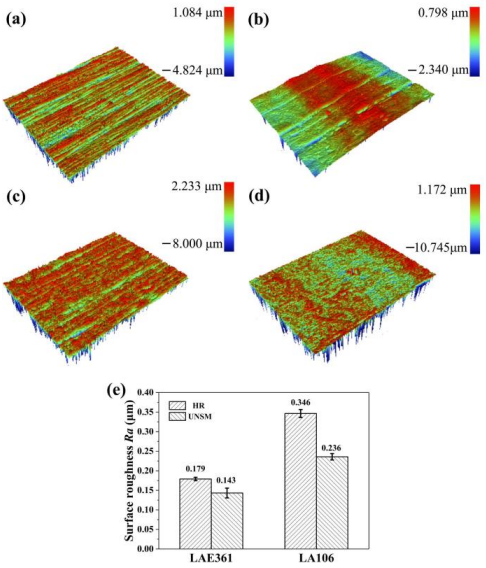

Figure 4. Three-dimensional morphology of LAE361 Mg-Li alloy (**a**,**b**) and LA106 Mg-Li alloy (**c**,**d**) and responding surface roughness (Ra) (**e**) before and after the UNSM treatment.

3.3. Texture Evolution

LAE361 Mg-Li alloy is mainly composed of the α phase, whereas LA106 Mg-Li alloy is composed of the α and β phases. Therefore, the {0002} and {10$\bar{1}$0} pole figures are required to analyze the texture in the α phase, whereas the {200} and {110} pole figures are used to analyze the texture in the β phase. Figure 5 shows the pole figures of the α phase of the two Mg-Li alloys before and after the UNSM treatment. The α phase of both Mg-Li alloys exhibits a typical basal texture. After the UNSM treatment, LAE361 Mg-Li alloy formed the {0002}<11$\bar{2}$0> basal texture with an intensity of 3.3 along with the {10$\bar{1}$2}<10$\bar{1}$0> texture (Figure 5). The UNSM treatment significantly reduced the intensity of the basal textures of the HR LAE361 Mg-Li alloy. While the basal textures were weakened, the intensity of the non-basal textures increased slightly. The scattering degree of the LAE361 Mg-Li alloy {0002} pole figure increased in the rolling direction (RD) and decreased in the transverse direction (TD). The α phase of the hot-rolled LA106 Mg-Li alloy exhibited {0002}<11$\bar{2}$0> texture with an intensity of 2.6. After the UNSM treatment, LA106 Mg-Li alloy mainly formed the {0002}<11$\bar{2}$0> (intensity of 2) and the {10$\bar{1}$2}<10$\bar{1}$0> textures (Figure 5c,d). The texture intensity of the HR Mg-Li alloys decreased after the UNSM treatment.

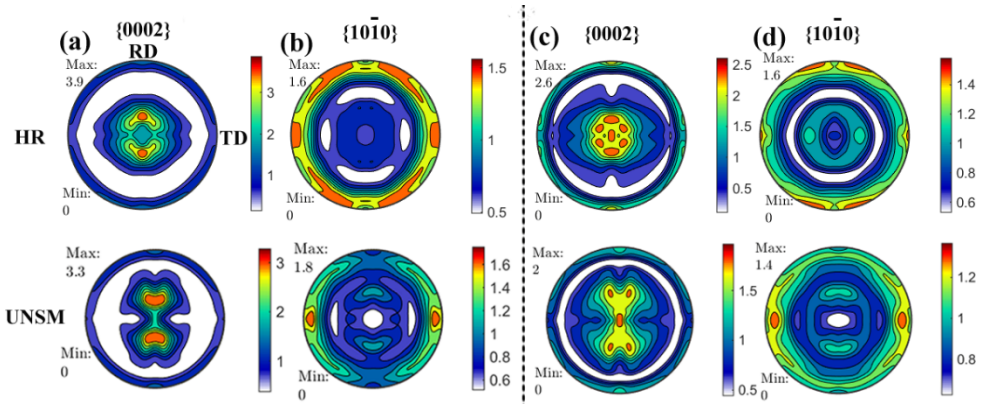

Figure 5. {0002} and {10$\bar{1}$0} pole figures of LAE361 Mg-Li alloy (**a**,**b**) and LA106 Mg-Li alloy (**c**,**d**) before and after the UNSM treatment.

Figure 6 shows the {200} and {110} pole figures of the β phase of LA106 before and after the UNSM treatment. The β phase of the hot-rolled LA106 Mg-Li alloy exhibited γ {111}<1$\bar{1}$2> and η fiber textures {011}<100>. After UNSM treatment, the LA106 Mg-Li alloy mainly exhibits α {111}<1$\bar{1}$0> and ε {001}<1$\bar{1}$0> linear texture. In other words, for LA106 Mg-Li alloy after UNSM treatment, the type of texture changes, but the strength of texture basically does not change.

3.4. Mechanical Behaviour

3.4.1. Microhardness

Severe deformation was observed on the surfaces of the LAE361 and LA106 Mg-Li alloys after UNSM, which affected the surface microhardness of the samples. Figure 7 shows the microhardness of the Mg-Li alloys before and after UNSM. Notably, the average surface microhardness values of the UNSM-treated LAE361 and LA106 samples were approximately 104 and 99.1 $HV_{0.05}$, respectively. The microhardness of LAE361 and LA106 samples improved by 17.5% and 39%, respectively, compared to the microhardness of the matrix samples (LAE361: ~88.5 $HV_{0.05}$, LA106: ~71.3 $HV_{0.05}$). Furthermore, as the distance from the surface increased, the microhardness gradually decreased. It became constant at a depth of approximately 350 μm.

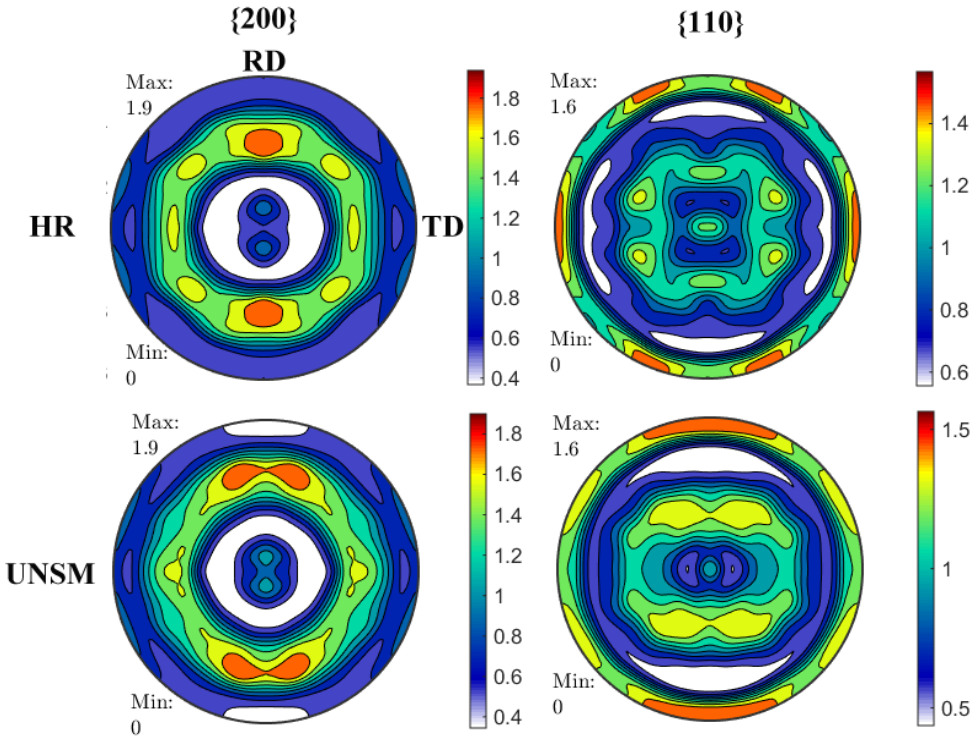

Figure 6. {200} and {110} pole figures of LA106 Mg-Li alloy before and after the UNSM treatment.

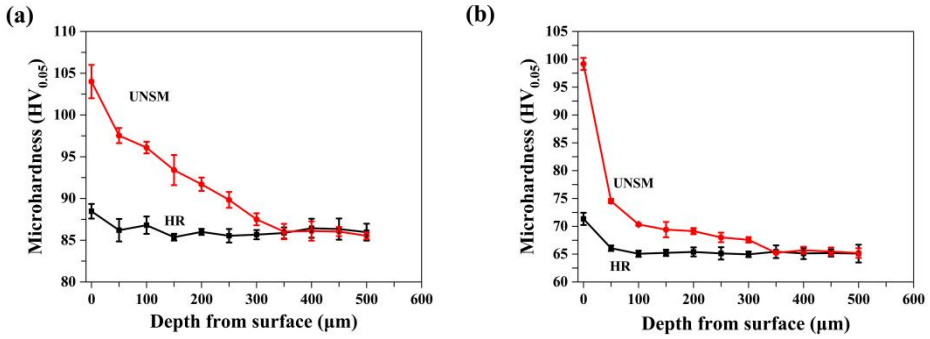

Figure 7. Microhardness distribution of the cross-sections of LAE361 Mg-Li alloy (**a**) and LA106 Mg-Li alloy (**b**) before and after UNSM treatment.

3.4.2. Tensile Mechanical Properties

The engineering stress–strain curves are shown in Figure 8. During the UNSM treatment, the surface of the Mg-Li alloy underwent SPD, leading to the refinement of the surface grains. Meanwhile, the dislocation density and grain boundary volume fraction increased. These results indicate that the UNSM treatment increased the tensile yield strength (TYS) and ultimate tensile strength (UTS) of the Mg-Li alloy. The matrix samples of LAE361 and LA106 Mg-Li alloys exhibited a TYS of ~246 and 149 MPa, respectively. After the UNSM treatment, the TYS of LAE361 and LA106 Mg-Li alloys were ~261 and 154 MPa, respectively. The UTS of the matrix samples of LAE361 and LA106 Mg-Li alloys were ~258 and 172 MPa, respectively. In contrast, that of the pieces after the UNSM treatment were 304 and 185 MPa, respectively. Moreover, the TYS and UTS of the pieces increased after the UNSM treatment. This increase was caused by the formation of an SPD layer on the surface of the alloys. The curve of the LA106 Mg-Li alloy showed jagged fluctuations after the UNSM treatment (Figure 8b). This phenomenon is called dynamic strain ageing (DSA) or the Portevin–Le Chatelier effect [24]. The material has sufficient time to alternately soften and harden at a lower strain rate during the deformation process, resulting in jagged fluctuations in the stress–strain curve.

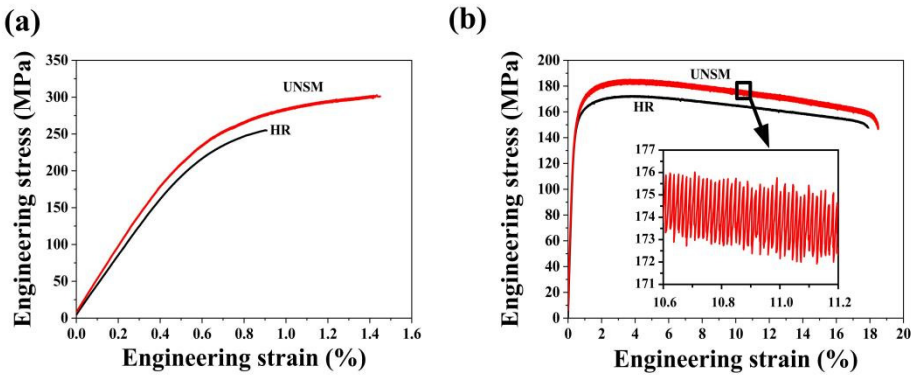

Figure 8. Engineering stress-strain curves of LAE361 Mg-Li alloy (**a**) and LA106 Mg-Li alloy (**b**) before and after UNSM treatment.

3.4.3. Fracture Analysis

Figure 9 shows the images of the fractured surfaces of LAE361 and LA106 Mg-Li alloys before and after UNSM. The fractured surface of LAE361 Mg-Li alloy exhibited a cleavage step, which appears as a brittle fracture, as shown in Figure 9a,b. Moreover, a river pattern and tear ridges appeared on the surface of the UNSM-treated surface. However, the plasticity of the surface improved slightly after the UNSM treatment, which may be related to the weakening of the basal textures and simultaneous twin deformation caused by the UNSM treatment. Figure 9c,d show the presence of dimples of different sizes in the fractures of the LA106 surface. The small dimples aggregated around the large dimples, and second-phase particles were observed inside the large dimples. On the UNSM-treated surface, the number of dimples increased along the direction of increasing distance from the surface, which is explained by the SPD formed on the surface layer.

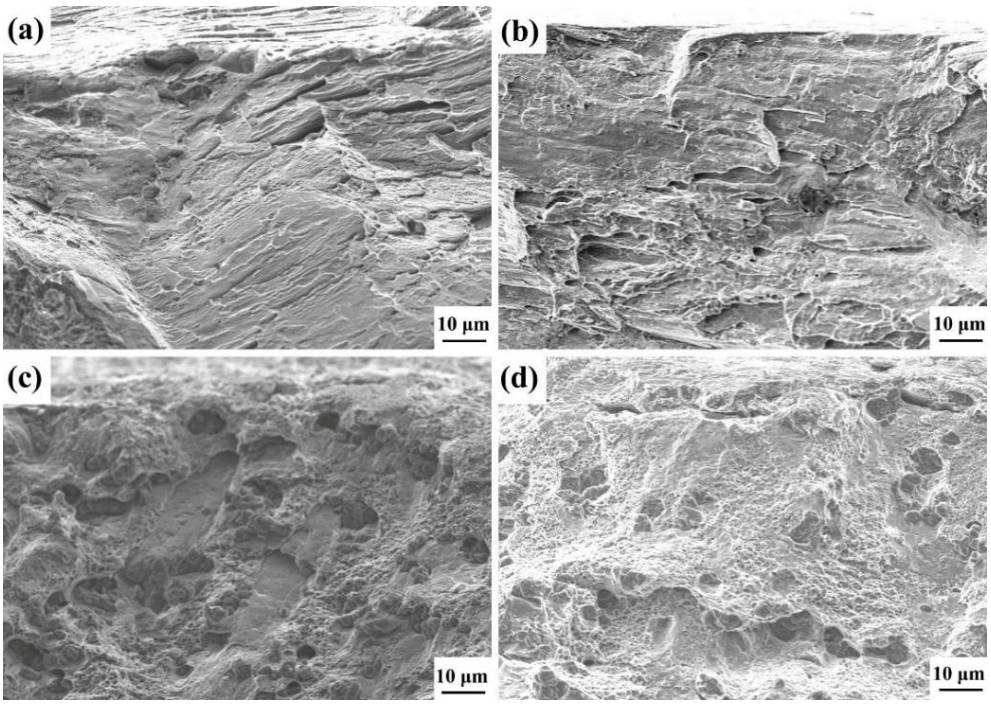

Figure 9. SEM images of the fractured surfaces of LAE361 Mg-Li alloy (**a**,**b**) and LA106 Mg-Li alloy (**c**,**d**) before and after the UNSM treatment.

3.5. Corrosion Behaviour

3.5.1. Electrochemical Corrosion

Figure 10 shows the open circuit curves of the LAE361 and LA106 Mg-Li alloys immersed in 3.5 wt.% NaCl solution. The average open-circuit potentials of LAE361 and LA106 Mg-Li alloys before the UNSM treatment were −1.604 and −1.644 V, respectively, and after the treatment were −1.602 V and −1.592 V, respectively.

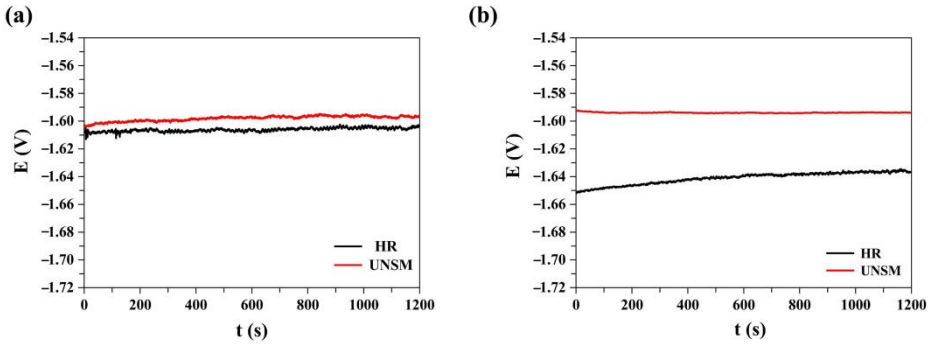

Figure 10. The open circuit curves of LAE361 Mg-Li alloy (**a**) and LA106 Mg-Li alloy (**b**) before and after the UNSM treatment in 3.5 wt.% NaCl solution at RT.

Figure 11 shows the Nyquist plots of LAE361 and LA106 Mg-Li alloys immersed in 3.5 wt.% NaCl solution. Based on the diameter of the capacitive reactance arc, it can be inferred that after the UNSM treatment, the corrosion resistance of LAE361 Mg-Li alloy improved. However, the corrosion resistance of LA106 Mg-Li alloy deteriorated significantly after the treatment. The Nyquist plots of EIS were fitted by using the ZSimpWin 3.10 software with the equivalent circuit $R_s\_(Q\_R_{ct})|(L\_R_1)$ [25]. The fitting parameters are summarized in Table 2. In the equivalent circuit, R_S and R_{ct} represent solution resistance and charge transfer resistance. Resistor R_1 and inductor L respectively stand for resistance and inductance, which are used to describe the low-frequency inductance loop and are generally related to the nucleation of localized corrosion and dissolution (breakdown of the oxide layer) or adsorption processes [26,27]. A constant phase element (*CPE*, denoted Q) is used instead of the ideal double-layer capacitance (C_{d1}) to address the non-ideal behaviour of the bilayer due to surface inhomogeneities, roughness and adsorption effects. Meanwhile, n is designated as the dispersion coefficient of Q. When the n value is 1, Q can be considered as a capacitor; when the n value is zero, Q can act as a resistance. The polarization resistance R_p is calculated as $R_p = R_1 + R_{ct}$. The polarization resistance R_p of LAE361 Mg-Li alloy was 1308.2 Ω cm^2 after UNSM, greater than that of the matrix sample (645.7 Ω cm^2), which shows that the corrosion resistance of LAE361 Mg-Li alloy improved by UNSM. However, the R_p of LA106 decreased from 631.4 to 106.7 Ω cm^2. Hence, the UNSM treatment was not conducive to the corrosion resistance of the duplex phase LA106 Mg-Li alloy.

Figure 12 shows the potential polarization curves of the LAE361 and LA106 Mg-Li alloys in 3.5 wt.% NaCl solution. The corresponding corrosion potential (E_{corr}) and corrosion current densities (i_{corr}) are listed in Table 3. The corrosion current density of LAE361 Mg-Li alloy decreased from 123.7 to 87.5 μA cm^{-2} after UNSM, while the corrosion current density of LA106 Mg-Li alloy increased from 119.3 to 345.6 μA cm^{-2}. The corrosion potential of LAE361 Mg-Li alloy increased from −1.57 to −1.56 V after UNSM, and the corrosion potential of LA106 Mg-Li alloy increased from −1.58 to −1.47 V.

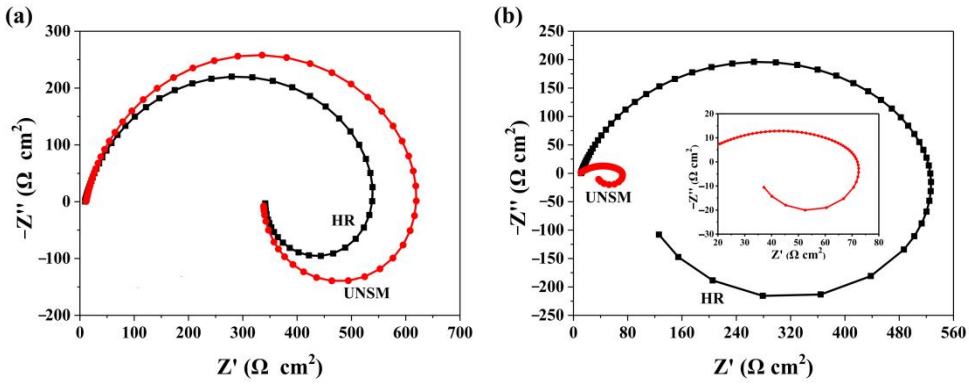

Figure 11. Nyquist plots of LAE361 Mg-Li alloy (**a**) and LA106 Mg-Li alloy (**b**) before and after the UNSM treatment in 3.5 wt.% NaCl solution at RT.

Table 2. EIS parameters obtained from the fitted equivalent circuit.

Sample	LAE361		LA106	
Processing state	HR	UNSM	HR	UNSM
R_S (Ω cm^2)	9.6	11.4	11.3	9.6
CPE (S cm^{-2} s^n)	3.50×10^{-5}	3.02×10^{-5}	7.97×10^{-5}	1.22×10^{-3}
n	0.85	0.87	0.81	0.46
R_{ct} (Ω cm^2)	565.3	635.4	528.1	67.9
L (H cm^2)	327.7	527.5	2624.0	257.2
R_1 (Ω cm^2)	80.4	672.8	103.3	38.8
R_p (Ω cm^2)	645.7	1308.2	631.4	106.7

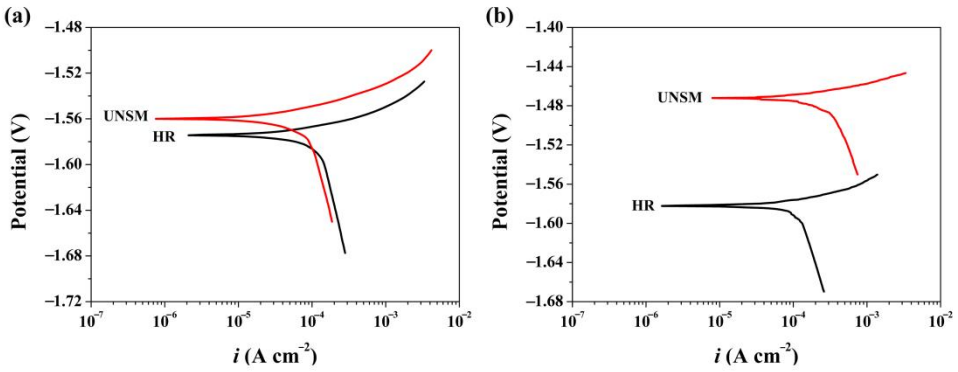

Figure 12. Potentiodynamic polarization curves of LAE361 Mg-Li alloy (**a**) and LA106 Mg-Li alloy (**b**) before and after the UNSM treatment in 3.5 wt.% NaCl solution at RT.

Table 3. E_{corr} and i_{corr} of LAE361 and LA106 Mg-Li alloys before and after the UNSM treatment.

Sample	LAE361		LA106	
Processing state	HR	UNSM	HR	UNSM
E_{corr} (vs SCE)/V	−1.57	−1.56	−1.58	−1.47
i_{corr}/(μA cm^{-2})	123.7	87.5	119.3	345.6

3.5.2. Hydrogen Evolution Test

The samples were immersed in 3.5 wt. % NaCl solution at RT for 48 h. The variations in the hydrogen evolution volumes and rates with time are shown in Figure 13. The hydrogen evolution volumes of the LAE361 Mg-Li alloy before and after UNSM were about 19.3 and 11.4 mL, respectively. The hydrogen evolution volumes of the LA106 Mg-Li alloy before and after UNSM were approximately 19.6 and 31.0 mL, respectively. These results show

that after UNSM, the hydrogen evolution volume of the LAE361 Mg-Li alloy decreased, while that of the LA106 Mg-Li alloy increased.

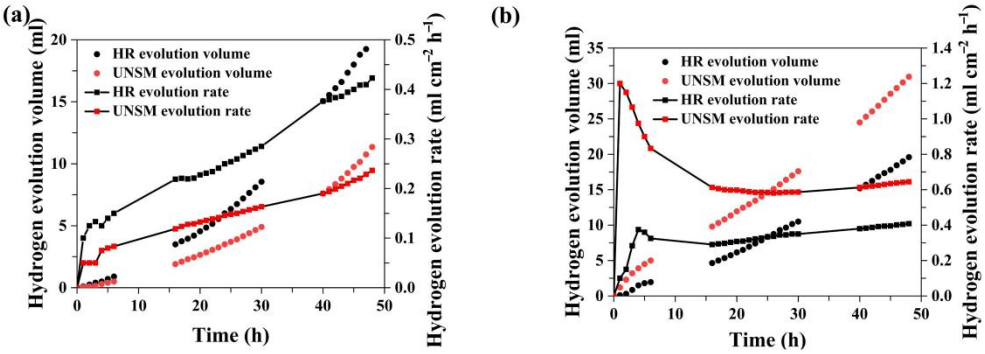

Figure 13. Variation in the hydrogen evolution volumes and rates of LAE361 Mg-Li alloy (**a**) and LA106 Mg-Li alloy (**b**) with time.

The hydrogen evolution rates of the LAE361 Mg-Li alloy before and after UNSM were 0.42 and 0.24 mL cm^{-2} h^{-1}, respectively. The hydrogen evolution rates of the LA106 Mg-Li alloy before and after UNSM were 0.41 and 0.64 mL cm^{-2} h^{-1}, respectively. These results are consistent with those obtained from the electrochemical tests. The corrosion resistance of LAE361 Mg-Li alloy improved after UNSM, while that of LA106 Mg-Li alloy deteriorated.

Figure 14 shows the surface morphologies of LAE361 and LA106 Mg-Li alloys after immersion. As shown in Figure 14a,b, LAE361 Mg-Li alloy exhibited reduced surface corrosion after UNSM, while LA106 Mg-Li alloy exhibited increased surface corrosion with large corrosion pits on the surface. It was inferred that the UNSM treatment improved the corrosion resistance of LAE361 Mg-Li alloy but impaired the corrosion resistance of LA106 Mg-Li alloy. This observation is consistent with the results of the hydrogen evolution test.

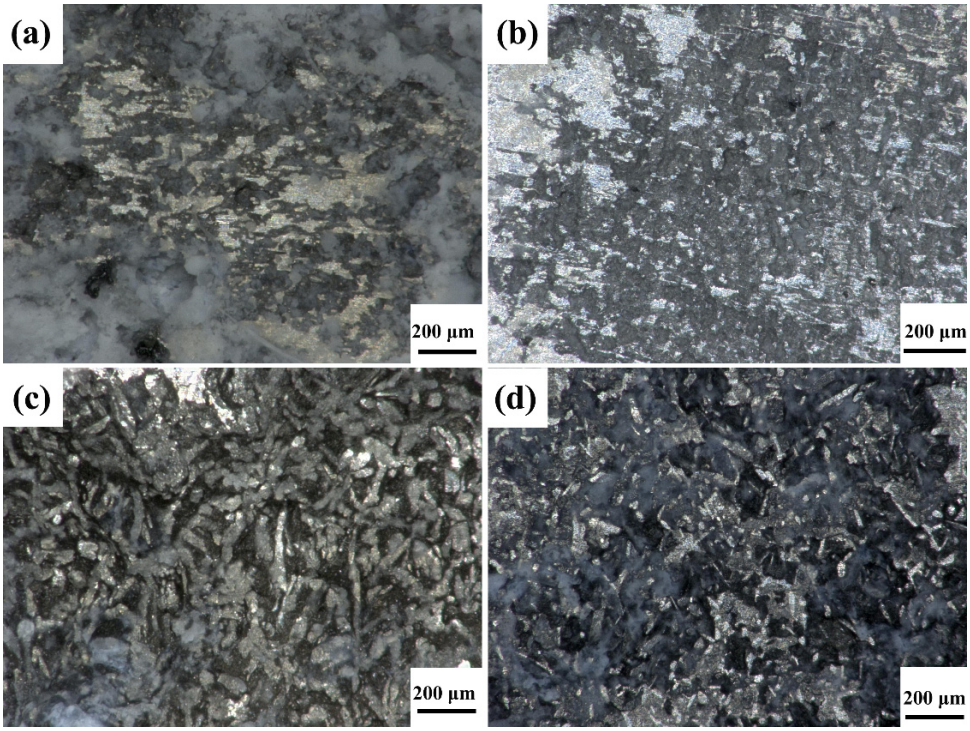

Figure 14. Surface morphologies of LAE361 Mg-Li alloy (**a**,**b**) and LA106 Mg-Li alloy (**c**,**d**) before and after the UNSM treatment in 3.5 wt.% NaCl solution for 48 h.

4. Discussion

After the UNSM treatment, the phase composition of LAE361 and LA106 Mg-Li alloys remained unchanged. At the same time, there was no apparent phase change in the Mg-Li alloys according to their XRD patterns. However, the intensity of the diffraction peak of the α-Mg phase of LAE361 and LA106 Mg-Li alloys significantly decreased, while the peak width broadened slightly. This may have occurred due to the generation of internal stresses, such as stacking fault energy and twinning [28]. As the material surface was highly strained, SPDs and grain refinements reduced the peak intensities while broadening the peak widths [29]. From the microstructure analysis, it can be inferred that the UNSM treatment induced high strain in the surface layers of the LAE361 and LA106 Mg-Li alloys, which caused SPD and grain refinement.

In contrast to SP, the surface roughness (Ra) of LAE361 and LA106 Mg-Li alloys was reduced by approximately 20% and 32% by UNSM treatment. It is known that a lower roughness value prevents the formation of cracks and reduces the actual contact area with the corrosion medium, which in return reduces the corrosion rate. However, because of the gradient in the plastic strain in the direction of depth, SPD on the surface may result in different degrees of grain refinement during the UNSM treatment. According to the classical Hall–Petch relationship [30], the microhardness increases as the grain size decreases. Therefore, the increased microhardness of the samples by UNSM may be due to the grain refinement and work hardening. Furthermore, the UNSM-treated specimens exhibited higher strength and better corrosion resistance.

4.1. Analysis of Tensile Properties

The strength and ductility of the material exhibited an inverse relationship. When the strength increases, the ductility will decrease significantly. Overcoming this strength–ductility trade-off is a significant challenge in developing metallic materials [12]. Refining the grain to nanometer scale is an effective strategy to increase the strength of metals, because the grain boundaries (GBs) in nanocrystalline metals and alloys can effectively block the dislocation motion [10].

From the tensile test results, it was observed that the UNSM treatment increased the strength of LAE361 and LA106 Mg-Li alloys and also improved the plasticity slightly. As shown in Figure 2c,e, several twins were observed in the microstructure of the alloy surface. From Figure 5a,b, it can be inferred that during the UNSM process, the α phase on the surface of the LAE361 Mg-Li alloy underwent twin deformation in addition to the basal slip. In addition, the elastic section of LAE361 Mg-Li alloy treated by UNSM has a high slope, which means a high elastic modulus. The reasons for this may be as follows: grain refinement, high residual compressive stress, and dislocation strain strengthening [23]. Meanwhile, twins were also observed in the α phase of LA106 Mg-Li alloy (Figure 2d,f); therefore, the α phase of LA106 Mg-Li alloy also underwent basal slip and twin deformation during the UNSM process (Figure 5c,d). Since the α phase was less deformable than the β phase, plastic deformation was mainly induced in the β phase with a sufficient slip system. Therefore, more SPDs occurred in the β phase. Moreover, the texture composition of LA106 Mg-Li alloy changed after the UNSM treatment (Figure 6). The β phase of LA106 Mg-Li alloy exhibited dislocation slips during the UNSM process. Previous studies have shown that dynamic recovery is likely to occur in the β phase with high stacking fault energy, because it is prone to cross-slip [31]. Generally, the appearance of the α-fibre texture is related to recovery. Therefore, the β phase may recover during deformation. This explains the increase in the plasticity of LA106 Mg-Li alloy. The elastic segment of LA106 Mg-Li alloy does not change after UNSM. The reason is that LAE361 Mg-Li alloy has α phase structure and LA106 Mg-Li alloy has α + β phase structure. The grain refinement of Mg alloy with α phase is more prominent, so the influence on the elastic modulus is not prominent [23].

4.2. Corrosion Resistance Analysis

According to Figure 11, the corrosion current density represents the corrosion speed, which is a dynamic concept, and the corrosion potential represents the corrosion tendency, which is a thermodynamic concept. The corrosion potential of LAE361 Mg-Li alloy by UNSM treatment did not change significantly, meaning that its corrosion tendency was unchanged. The corrosion current density of LAE361 Mg-Li alloy decreased by UNSM, indicating that its corrosion rate also decreased. The corrosion potential of LA106 Mg-Li alloy increased by UNSM, indicating its increased corrosion resistance. However, the corrosion current density of LA106 Mg-Li alloy increased significantly by UNSM, which shows that the alloy was corroded easily. Once corrosion occurred, the corrosion rate increased. These results showed that the UNSM treatment could improve the corrosion resistance of the single-phase LAE361 Mg-Li alloy. However, it was not conducive to the corrosion resistance of the duplex phases LA106 Mg-Li alloy.

Previous studies showed that surface roughness has a significant effect on the corrosion resistance of materials. The surface roughness of LAE361 and LA106 Mg-Li alloys decreased after UNSM treatment. Therefore, it was assumed that the corrosion resistance of both the alloys would increase. However, unlike the LAE361 Mg-Li alloy, the corrosion resistance of the LA106 Mg-Li alloy decreased. Xiang et al. [32] reported that the increased corrosion resistance of the LA51 alloy sheet after rolling was due to texture and twinning. Although the intensity of the basal textures in the LAE361 Mg-Li alloy decreased, several twins appeared in the α phase due to SPD on the surface layer, which may have helped improve its corrosion resistance. For the duplex phases LA106 Mg-Li alloy, due to more active Li elements, LA106 Mg-Li alloy more easily corroded. Meanwhile, the micro-galvanic corrosion between the duplex phases (α + β) makes the corrosion of LA106 Mg-Li alloy more complicated, which results in the phenomenon that the corrosion resistance decreases after UNSM treatment. First, the soft β phase was relatively easy to deform, and its potential was more negative than that of the α phase. The UNSM treatment led to the dislocation slip and grain refinement of the β phase, which introduced many dislocations, vacancies, and other defects, thereby increasing the practical collision between activated molecules. Then, galvanic corrosion between the α and β phase occurred quickly, and more serious pitting occurred, which led to a decrease in the corrosion resistance of the LA106 Mg-Li alloy.

It means that due to the difference in performance caused by the difference in microstructure, the influence of UNSM technology on the corrosion resistance of different Mg-Li alloys is distinct. Therefore, the use of UNSM technology for various phases of Mg-Li alloys needs to consider different processing parameters. On the other hand, UNSM technology has limitations in the processing of Mg-Li alloy with high Li element content. It is challenging to solve the problem of oxidation and corrosion in the processing process, resulting in a specific difference in surface characterization.

5. Conclusions

In this study, the microstructure, surface morphology, mechanical property, deformation mechanism, and corrosion property of LAE361 and LA106 Mg-Li alloys were studied before and after the UNSM treatment. The main conclusions of this study are as follows:

(1) After the UNSM treatment, the phase composition of LAE361 and LA106 Mg-Li alloys remained unchanged. An SPD layer was formed on the surface of samples, with several twins appearing in the α phase. Consequently, the grain structure of the alloys was refined.

(2) During the UNSM process, the α phase of the surface layer of LAE361 Mg-Li alloy underwent twin deformations in addition to the basal slips, which promoted dislocation slips on the non-basal surface. The α phase of the LA106 Mg-Li alloy mainly underwent twin deformations and basal slips, while dislocation slips occurred in the β phase.

(3) The surface microhardness of the LAE361 and LA106 Mg-Li alloys increased significantly after the UNSM treatment, and the depth of the hardening layer was 350 μm

for both alloys. Meanwhile, the strength and plasticity of the alloys improved, which was attributed to the formation of an SPD layer on the surface.

(4) The UNSM treatment was beneficial to the corrosion resistance of LAE361 Mg-Li alloy because of the appearance of several deformation twins in the α phase and lower surface roughness. The corrosion resistance of the duplex phases LA106 Mg-Li alloy significantly deteriorated because of more SPD on the β phase.

Author Contributions: Y.Z. and Y.L. conceived and designed the experiments; S.L. and Q.W. contributed to the sample preparation, mechanical property and corrosion behavior testing; Y.Z. and S.L. contributed to the data analysis; Y.Z. and S.L. wrote the paper. All authors have read and agreed to the published version of the manuscript.

Funding: The authors are grateful for the financial support of this research by the National Science Foundation of China under Grant 51801185, Special Research and Promotion Project of Henan Province, China, under Grant 182102210009, and the Training Program for Young Backbone Teachers of the Higher Education Institutions of Henan Province, China.

Institutional Review Board Statement: Not applicable.

Informed Consent Statement: Not applicable.

Data Availability Statement: Not applicable.

Acknowledgments: We are grateful for experimental equipment support by the Center of Advanced Analysis & Gene Sequencing, Zhengzhou University.

Conflicts of Interest: The authors declare no conflict of interest.

References

1. Zou, Y.; Zhang, L.; Li, Y.; Wang, H.T.; Liu, J.B.; Liaw, P.K.; Bei, H.B.; Zhang, Z.W. Improvement of mechanical behaviors of a superlight Mg-Li base alloy by duplex phases and fine precipitates. *J. Alloy. Compd.* **2018**, *735*, 2625–2633. [CrossRef]
2. Rahmatabadi, D.; Hashemi, R.; Tayyebi, M.; Bayati, A. Investigation of mechanical properties, formability, and anisotropy of dual phase Mg-7Li-1Zn. *Mater. Res. Express* **2019**, *6*, 106955. [CrossRef]
3. Pan, F.; Yang, M.; Chen, X. A Review on Casting Magnesium Alloys: Modification of Commercial Alloys and Development of New Alloys. *J. Mater. Sci. Technol.* **2016**, *32*, 1211–1221. [CrossRef]
4. Zeng, R.C.; Sun, L.; Zheng, Y.F.; Cui, H.Z.; Han, E.H. Corrosion and characterisation of dual phase Mg-Li-Ca alloy in Hank's solution: The influence of microstructural features. *Corros. Sci.* **2014**, *79*, 69–82. [CrossRef]
5. Guo, J.; Chang, L.; Zhao, Y.; Jin, Y. Effect of Sn and Y addition on the microstructural evolution and mechanical properties of hot-extruded Mg-9Li-3Al alloy. *Mater. Charact.* **2019**, *148*, 35–42. [CrossRef]
6. Morishige, T.; Obata, Y.; Goto, T.; Fukagawa, T.; Nakamura, E.; Takenaka, T. Effect of Al Composition on the Corrosion Resistance of Mg-14 mass% Li System Alloy. *Mater. Trans.* **2016**, *57*, 1853–1856. [CrossRef]
7. Su, Q.; Xu, J.; Li, Y.; Yoon, J.I.; Shan, D.; Guo, B.; Kim, H.S. Microstructural Evolution and Mechanical Properties in Superlight Mg-Li Alloy Processed by High-Pressure Torsion. *Materials* **2018**, *11*, 598. [CrossRef]
8. Maurya, R.; Siddiqui, A.R.; Balani, K. An environment-friendly phosphate chemical conversion coating on novel Mg-9Li-7Al-1Sn and Mg-9Li-5Al-3Sn-1Zn alloys with remarkable corrosion protection. *Appl. Surf. Sci.* **2018**, *443*, 429–440. [CrossRef]
9. Liu, G.; Wang, S.C.; Lou, X.F.; Lu, J.; Lu, K. Low carbon steel with nanostructured surface layer induced by high-energy shot peening. *Scr. Mater.* **2001**, *44*, 1791–1795. [CrossRef]
10. Fu, P.; Zhan, K.; Jiang, C. Micro-structure and surface layer properties of 18CrNiMo7-6 steel after multistep shot peening. *Mater. Des.* **2013**, *51*, 309–314. [CrossRef]
11. Liu, C.; Zheng, H.; Gu, X.; Jiang, B.; Liang, J. Effect of severe shot peening on corrosion behavior of AZ31 and AZ91 magnesium alloys. *J. Alloy. Compd.* **2019**, *770*, 500–506. [CrossRef]
12. Azhari, A.; Schindler, C.; Hilbert, K.; Godard, C.; Kerscher, E. Influence of waterjet peening and smoothing on the material surface and properties of stainless steel 304. *Surf. Coat. Technol.* **2014**, *258*, 1176–1182. [CrossRef]
13. Azhari, A.; Schindler, C.; Godard, C.; Gibmeier, J.; Kerscher, E. Effect of multiple passes treatment in waterjet peening on fatigue performance. *Appl. Surf. Sci.* **2016**, *388*, 468–474. [CrossRef]
14. Wang, H.; Huang, Y.; Zhang, W.; Ostendorf, A. Investigation of multiple laser shock peening on the mechanical property and corrosion resistance of shipbuilding 5083Al alloy under a simulated seawater environment. *Appl. Opt.* **2018**, *57*, 6300–6308. [CrossRef]
15. Zhang, R.; Zhou, X.; Gao, H.; Mankoci, S.; Liu, Y.; Sang, X.; Qin, H.; Hou, X.; Ren, Z.; Doll, G.L.; et al. The effects of laser shock peening on the mechanical properties and biomedical behavior of AZ31B magnesium alloy. *Surf. Coat. Technol.* **2018**, *339*, 48–56. [CrossRef]

16. Zhang, Y.; Lu, J.; Ren, X.; Yao, H. Effect of laser shock processing on the mechanical properties and fatigue lives of the turbojet engine blades manufactured by LY2 aluminum alloy. *Mater. Des.* **2009**, *30*, 1697–1703. [CrossRef]
17. Li, C.; Cui, W.; Zhang, Y. Surface self-nanocrystallization of α+β titanium alloy by surface mechanical grinding treatment. *Met. Mater. Int.* **2017**, *23*, 512–518. [CrossRef]
18. Huang, H.W.; Wang, Z.B.; Yong, X.P.; Lu, K. Enhancing torsion fatigue behaviour of a martensitic stainless steel by generating gradient nanograined layer via surface mechanical grinding treatment. *Mater. Sci. Technol.* **2013**, *29*, 1200–1205. [CrossRef]
19. Lu, K. Making strong nanomaterials ductile with gradients. *Science* **2014**, *345*, 1455–1456. [CrossRef]
20. Ye, C.; Telang, A.; Gill, A.; Wen, X.; Mannava, S.R.; Qian, D.; Vasudevan, V.K. Effects of Ultrasonic Nanocrystal Surface Modification on the Residual Stress, Microstructure, and Corrosion Resistance of 304 Stainless Steel Welds. *Met. Mater. Trans. A* **2018**, *49*, 972–978. [CrossRef]
21. Hou, X.; Qin, H.; Gao, H.; Mankoci, S.; Zhang, R.; Zhou, X.; Ren, Z.; Doll, G.L.; Martini, A.; Sahai, N.; et al. A systematic study of mechanical properties, corrosion behavior and biocompatibility of AZ31B Mg alloy after ultrasonic nanocrystal surface modification. *Mater. Sci. Eng. C* **2017**, *78*, 1061–1071. [CrossRef] [PubMed]
22. Amanov, A.; Penkov, O.V.; Pyun, Y.S.; Kim, D.E. Effects of ultrasonic nanocrystalline surface modification on the tribological properties of AZ91D magnesium alloy. *Tribol. Int.* **2012**, *54*, 106–113. [CrossRef]
23. Ye, H.; Sun, X.; Liu, Y.; Rao, X.X.; Gu, Q. Effect of ultrasonic surface rolling process on mechanical properties and corrosion resistance of AZ31B Mg alloy. *Surf. Coat. Technol.* **2019**, *372*, 288–298. [CrossRef]
24. Gupta, A.K.; Krishnamurthy, H.N.; Singh, Y.; Prasad, K.M.; Singh, S.K. Development of constitutive models for dynamic strain aging regime in Austenitic stainless steel 304. *Mater. Des.* **2013**, *45*, 616–627. [CrossRef]
25. Zou, Y.; Zhang, Z.; Liu, S.; Chen, D.; Wang, G.; Wang, Y.; Zhang, M.; Chen, Y. Ultrasonic-Assisted Electroless Ni-P Plating on Dual Phase Mg-Li Alloy. *J. Electrochem. Soc.* **2014**, *162*, C64–C70. [CrossRef]
26. Song, Y.; Shan, D.; Chen, R.; Han, E.H. Corrosion characterization of Mg–8Li alloy in NaCl solution. *Corros. Sci.* **2009**, *51*, 1087–1094. [CrossRef]
27. Szklarz, Z.; Bisztyga, M.; Krawiec, H.; Litynska-Dobrzynska, L.; Rogal, Ł. Global and local investigations of the electrochemical behavior the T6 heat treated Mg–Zn–RE magnesium alloy thixo-cast. *Appl. Surf. Sci.* **2017**, *405*, 529–539. [CrossRef]
28. Amanov, A.; Urmanov, B.; Amanov, T.; Pyun, Y. Strengthening of Ti-6Al-4V alloy by high temperature ultrasonic nanocrystal surface modification technique. *Mater. Lett.* **2017**, *196*, 198–201. [CrossRef]
29. Ahn, D.H.; Kim, W.; Kang, M.; Park, L.J.; Lee, S.; Kim, H.S. Plastic deformation and microstructural evolution during the shock consolidation of ultrafine copper powders. *Mater. Sci. Eng. A* **2015**, *625*, 230–244. [CrossRef]
30. Hansen, N. Hall–Petch relation and boundary strengthening. *Scr. Mater.* **2004**, *51*, 801–806. [CrossRef]
31. Sun, Y.; Wang, R.; Ren, J.; Peng, C.; Cai, Z. Microstructure, texture, and mechanical properties of as-extruded Mg-xLi-3Al-2Zn-0.2Zr alloys (x = 5, 7, 8, 9, 11 wt%). *Mater. Sci. Eng. A* **2019**, *755*, 201–210. [CrossRef]
32. Xiang, Q.; Jiang, B.; Zhang, Y.; Chen, X.-B.; Song, J.; Xu, J.; Fang, L.; Pan, F. Effect of rolling-induced microstructure on corrosion behaviour of an as-extruded Mg-5Li-1Al alloy sheet. *Corros. Sci.* **2017**, *119*, 14–22. [CrossRef]